Cooperative Relative UAV Attitude Estimation Using DOA and RF Polarization

Jon W. Wallace *Senior Member, IEEE*, Attiya Mahmood, *Student Member, IEEE*,
Michael A. Jensen *Fellow, IEEE*, Rashid Mehmood *Member, IEEE*

***Abstract*—Relative unmanned aerial vehicle attitude is estimated using only on-board radio-frequency signaling. The method uses a direction-of-arrival (DOA) vector estimate to determine two degrees-of-freedom (DOFs), a polarimetric narrowband multiple-input multiple-output (MIMO) channel estimate to specify the third DOF to within a 180° ambiguity, and one of several potential methods for ambiguity resolution. Simulation results demonstrate that the method accurately determines aircraft attitude, with errors proportional to DOA and MIMO channel estimate errors. This approach is useful for cooperative navigation when external navigation aids are not available, such as in GPS-denied environments.**

***Index Terms*—Unmanned aerial vehicles, Pose estimation, Direction-of-arrival estimation, MIMO systems, Relative attitude estimation, Cooperative navigation**

I. Introduction

ATTITUDE estimation in unmanned aerial vehicles (UAVs) enables proper stability, control, and navigation and ensures the success of imaging and tracking missions. Aircraft attitude consists of three degrees-of-freedom (DOFs), specified using yaw, pitch, and roll (YPR) angles, orientation matrices, or quaternions [1]. A variety of approaches exist for estimating attitude, with the appropriate selection depending on size, weight, cost, and accuracy constraints. This paper focuses on the problem of *relative attitude* estimation, whose solution can serve as a required input for cooperative navigation and control as well as collective localization in robot swarms [2]–[6]. Relative attitude of ground-based robots only requires bearing information, which can be obtained with sonar, laser sensing, cameras, etc. However, obtaining the full three-DOF relative attitude of UAVs is more challenging.

An obvious solution for obtaining attitude information is for the UAVs to individually estimate their attitude with respect to a common frame of reference (such as the earth) and then share that information wirelessly. Traditionally, manned and unmanned aircraft use inertial tracking along with compass information to determine attitude [7]–[9]. However, disadvantages of these techniques for UAVs include poor accuracy of small low-cost inertial sensors, accelerometer error from high accelerations, gyroscope accumulation error, and magnetometer error due to local disturbances of the earth's magnetic field. Alternatively, it is possible to estimate attitude by optically tracking visual references, such as the horizon, sun, stars, or landmarks [10]–[14]. While optical methods have demonstrated acceptable accuracy, they are limited to conditions with sufficient visibility.

Global positioning satellite (GPS) technology overcomes most difficulties associated with other technologies, allowing estimation of both location and attitude using multiple receive antennas [15]–[18]. However, GPS signals are susceptible to obstruction of the required satellites or intentional jamming, and typical GPS-only methods provide only two of the three attitude DOFs. Full three-DOF attitude estimation is possible by employing widely separated GPS receive antennas [15], but such a configuration is not appropriate for many smaller UAVs. For these reasons, fusion methods have been developed that combine GPS with existing non-GPS sensors to overcome limitations and improve performance [19], [20].

Given the drawbacks of existing approaches, particularly for GPS-denied scenarios [21], an attractive alternative is to use radio-frequency (RF) techniques for attitude determination, possibly leveraging existing communications radios and eliminating additional sensors. RF methods have a long history of use for navigation in aviation, with systems such as very high frequency (VHF) omnidirectional range and non-directional beacon (NDB) stations still in active use. Although these systems are designed for localization, the work in [22], [23] demonstrates the use of low-frequency (LF) radio waves (available from NDBs and amplitude modulation (AM) radio stations) for three-DOF attitude estimation by exploiting the polarization of LF signals. The work in [24] shows the use of monopulse methods to estimate the three-DOF attitude of a satellite using RF signals from at least two ground stations. In [25], multiple antennas on both the UAV and a ground station enable three-DOF attitude estimation by estimating the relative path lengths between all antenna pairs. Finally, satellite attitude estimation using multiple low earth orbit satellites is treated in [26]. However, the need for dedicated ground or space-based equipment, the susceptibility to signal obstruction and outage, and in some cases the need for ultrawideband (UWB) signals and station/aircraft proximity makes these methods impractical for many applications.

Some methods have appeared that provide relative attitude estimates without the need for dedicated ground or space equipment. The technique described in [27] estimates the relative attitude of two spacecraft using at least two transmit antennas on one vehicle and three receive antennas on the other based on a method similar to that in [25], but accuracy requires UWB signaling and vehicle proximity. The methods in [28]

J. Wallace is with Lafayette College, Easton, PA, e-mail: wall@ieee.org
M. Jensen is with the Electrical and Computer Engineering Department, Brigham Young University, Provo, UT, e-mail: jensen@byu.edu
A. Mahmood and R. Mehmood are with Wavetronix, LLC, Provo, UT, e-mail: attiya.mahmood@wavetronix.com, r.mehmood@ieee.org

TABLE I
MATHEMATICAL NOTATION

Notation	Description	Equivalent in [36]
$\mathbf{r}$	Vector	$[r]$
$\hat{r}$	Unit vector	$[a_r]$
$\mathbf{M}$	Matrix or tensor	$[M]$
$\mathbf{M}^\dagger$	Matrix transpose of $\mathbf{M}$	$[M]$
$\mathbf{r}_\mathrm{A}$	Vector in frame A	$[r]^A$
$\mathbf{M}^\mathrm{A}_\mathrm{B}$	Coordinate transformation A $\rightarrow$ B	$[M]^{BA}$

and [29] use narrowband direction finding for relative attitude estimation but offer only two DOFs, requiring use of GPS signals or a magnetometer to obtain the third. Other related work employs radio ranging combined with optical direction finding and attitude estimation for space missions [30] or uses multiple passive RF identification (RFID) tags to estimate an object's attitude [31]. In [32], a method is presented that fuses data from inertial measurement units (IMUs), magnetometers, downward looking cameras, and RF ranging to provide high quality estimation of relative UAV pose. Similarly, the work in [33] provides a method for position, velocity, and attitude estimation for a group of miniature air vehicles by combining IMU, range, and bearing information of nearest neighbors. Unfortunately, these existing methods do not provide a unified RF method that can estimate relative three-DOF attitude using moderate bandwidth for small UAVs at arbitrary range without requiring additional sensors.

The purpose of this work is to show that by increasing the complexity of RF resources on a UAV (multiple antennas and multichannel radios), full relative attitude of two UAVs can be estimated without the need of any non-RF sensors. The method uses direction finding to obtain two attitude DOFs and narrowband, multi-polarization multiple-input multiple-output (MIMO) channel estimates to resolve the third. The method has the advantages over existing polarization-based RF attitude estimation [22], [23] that no ground-based infrastructure is required, that antennas operating at UHF and above are likely already to be available on UAVs, and that the antennas may be smaller than those required for LF systems. While initial simulation results based on this algorithm appear in prior work [34], [35], these reports omit mathematical derivation, algorithm description, and the detailed simulation results provided in this work. These simulation results demonstrate that the algorithm provides accurate attitude estimates, with errors being closely tied to the accuracy of the direction finding and MIMO channel estimates.

Table I defines the key mathematical notation adopted in this paper. The framework for orthogonal coordinate systems and transformations is equivalent to that found in [36], but we use alternate notation more typical of signal processing and electromagnetics literature. For those more familiar with the conventions in [36], Table I shows how to translate notation.

II. PROBLEM GEOMETRY

In this paper we adopt the scenario for relative attitude estimation found in [21] and depicted in Fig. 1. The *tracking* UAV (UAV^T) currently performs some operation (such as imaging of a ground target), and this UAV must be replaced

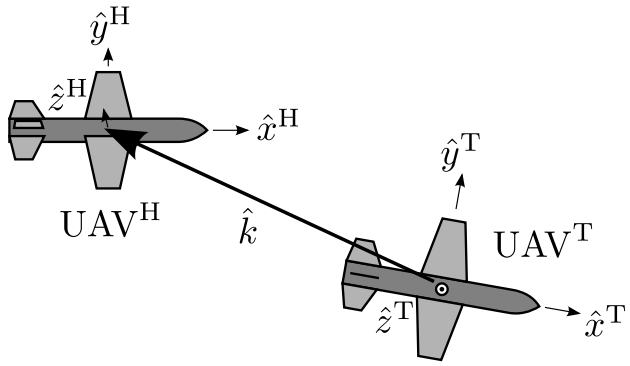

Fig. 1. Problem scenario showing how local right-hand coordinate systems are defined for tracking (T) and handoff (H) UAVs. The vector $\hat{k}$ gives the direction-of-arrival (DOA) at the handoff UAV for a signal transmitted from the tracking UAV.

by a *handoff* UAV (UAV^H) that takes over the operation. Successful handoff requires that the handoff UAV learn its three-DOF attitude relative to that of the tracking UAV. We could pose the problem as UAV^H directly estimating the required rotation (YPR) angles to align itself with UAV^T. However, rotation angles depend on the order of rotation and therefore do not specify attitude unambiguously. Furthermore, coordinate transformations based on YPR angles can be complicated, leading to a difficult estimation problem.

To avoid these difficulties, we instead take an orientation matrix approach by defining the attitude of each UAV in terms of three unit vectors that form a local right-hand orthogonal coordinate system (or *frame*), as depicted in Fig. 1. As there are several frames involved, we use the general notation

$$(\hat{x}^\mathrm{A}_\mathrm{B}, \hat{y}^\mathrm{A}_\mathrm{B}, \hat{z}^\mathrm{A}_\mathrm{B}) \tag{1}$$

as orthogonal unit vectors defining a Cartesian frame, where the subscript 'B' indicates the frame used as the *basis* for the vector elements and the superscript 'A' specifies the new frame defined by these vectors. No subscript means that the vector elements are in terms of the *global* basis vectors $(\hat{x}, \hat{y}, \hat{z})$ which could, for example, refer to directions of increasing longitude, latitude, and altitude. Frame $\mathrm{A} \in \{\mathrm{T}, \mathrm{H}\}$ indicates the tracking and handoff UAV body frame, respectively, where $\hat{x}^\mathrm{A}$, $\hat{y}^\mathrm{A}$, and $\hat{z}^\mathrm{A}$ are directions of the nose, left wing, and up from the fuselage, respectively, expressed in the global frame. Note that the frame and basis labels can also be identical, such as $(\hat{k}^\mathrm{A}_\mathrm{A}, \hat{v}^\mathrm{A}_\mathrm{A}, \hat{u}^\mathrm{A}_\mathrm{A})$, which indicates an alternate frame for A defined using the underlying Cartesian basis $(\hat{x}^\mathrm{A}, \hat{y}^\mathrm{A}, \hat{z}^\mathrm{A})$. When Cartesian unit vectors have the same subscript and superscript, they are simply elementary vectors, such as $\hat{z}^\mathrm{A}_\mathrm{A} = [0\ 0\ 1]^\dagger$. When needed, roll, pitch, and yaw are defined as positive rotation angles according to the right-hand rule about the $\hat{x}^\mathrm{A}$, $\hat{y}^\mathrm{A}$, and $\hat{z}^\mathrm{A}$ axes, respectively.

To simplify shifting from one frame to another we define $\mathbf{M}^\mathrm{A}_\mathrm{B}$ to be the transformation matrix from A to B that satisfies

$$\mathbf{r}_\mathrm{B} = \mathbf{M}^\mathrm{A}_\mathrm{B}\mathbf{r}_\mathrm{A}, \tag{2}$$

where $\mathbf{r}_\mathrm{A}$ and $\mathbf{r}_\mathrm{B}$ are the same vector defined in terms of the bases of frames A and B respectively. We have

$$\mathbf{M}^\mathrm{A}_\mathrm{B} = \left[\hat{x}^\mathrm{A}_\mathrm{B}\ \hat{y}^\mathrm{A}_\mathrm{B}\ \hat{z}^\mathrm{A}_\mathrm{B}\right] = \left[\hat{x}^\mathrm{B}_\mathrm{A}\ \hat{y}^\mathrm{B}_\mathrm{A}\ \hat{z}^\mathrm{B}_\mathrm{A}\right]^\dagger. \tag{3}$$

Note that $\mathbf{M}_{\mathrm{A}}^{\mathrm{B}} = (\mathbf{M}_{\mathrm{A}}^{\mathrm{B}})^{-1} = (\mathbf{M}_{\mathrm{B}}^{\mathrm{A}})^{\dagger}$ since we use orthonormal basis vectors.

III. Problem Solution

Before tackling the solution, let us first state assumed knowledge (inputs) and capabilities of the UAV systems:

1) An estimate of the MIMO channel ($\mathbf{H}_{\mathrm{meas}}$) between the tracking and handoff UAV arrays is available. Sending training symbols in one direction requires time $t_{\mathrm{meas}} = N_T/f_s$, where N_T is the number of transmit antennas and f_s is the symbol rate. It should be ensured that $1/t_{\mathrm{meas}}$ is large compared to the rate change of relative attitude.
2) At least one UAV has estimates of $\hat{k}_{\mathrm{T}}^{\mathrm{T}}$ and $\hat{k}_{\mathrm{H}}^{\mathrm{H}}$, which represent the direction-of-arrival (DOA) vector in each UAV local frame. This local DOA information does not require GPS, since UAVs can use arrays for direction finding [37], [38].
3) UAVs have knowledge of the complex (amplitude and phase) polarimetric far-field radiation patterns of their antenna arrays over the complete radiation sphere. Although this detailed knowledge would be sufficient to estimate and/or correct antenna phase center differences, such operations are not required in our solution.
4) A data channel exists between the UAVs to allow required information (the MIMO channel estimate, local DOA, antenna patterns) to be sent to the processing UAV node. This channel would also be used to send the resulting attitude estimate to the other UAV.
5) All inputs to the algorithm (MIMO channel and local DOA estimates at the two UAVs) are synchronized in time. If the MIMO channel is used for DOA estimation (Section IV-F), the two DOA estimates and the MIMO channel are inherently synchronized. If a unified DOA/MIMO channel estimation procedure is not used, any relative delay in DOA and MIMO estimates will increase attitude estimation errors.

Assumption 3 may be difficult to meet in practice, requiring patterns to be carefully measured in an anechoic chamber or in the air. Unfortunately, these patterns may be corrupted by moving control surfaces, changing payload on the outside of the UAV, and multipath effects. Although beyond the scope of this first treatment, we expect that careful transformation or processing of MIMO channel information will lead to algorithms that require less detailed knowledge and are more robust to pattern uncertainty.

For analytical convenience, we assume that no estimation error exists in the local DOA estimates or in the polarimetric MIMO channel estimates used in the following derivation. However, both DOA and channel estimation error *are* included in the simulations in Section IV.

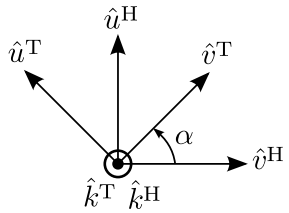

Fig. 2. The KVU reference frames of the tracking and handoff UAVs are related by a simple rotation of angle α about the common DOA vector. Thus, a vector in the handoff frame must be rotated by $-\alpha$ to represent it in the tracking frame.

A. Relating Frames With DOA Information

We begin by defining a local *KVU frame* in each UAV local frame by the unit vector triad $(\hat{k}_{\mathrm{A}}^{\mathrm{A}}, \hat{v}_{\mathrm{A}}^{\mathrm{A}}, \hat{u}_{\mathrm{A}}^{\mathrm{A}})$ where

$$\hat{u}_{\mathrm{A}}^{\mathrm{A}} = \begin{cases} (\hat{z}_{\mathrm{A}}^{\mathrm{A}} \times \hat{k}_{\mathrm{A}}^{\mathrm{A}})/\|\hat{z}_{\mathrm{A}}^{\mathrm{A}} \times \hat{k}_{\mathrm{A}}^{\mathrm{A}}\| & \text{for } \hat{k}_{\mathrm{A}}^{\mathrm{A}} \neq \hat{z}_{\mathrm{A}}^{\mathrm{A}} \\ \hat{x}_{\mathrm{A}}^{\mathrm{A}} & \text{otherwise} \end{cases} \tag{4}$$

$$\hat{v}_{\mathrm{A}}^{\mathrm{A}} = \hat{u}_{\mathrm{A}}^{\mathrm{A}} \times \hat{k}_{\mathrm{A}}^{\mathrm{A}}, \tag{5}$$

and $\mathrm{A} \in \{\mathrm{T}, \mathrm{H}\}$. The KVU unit vectors are analogous to spherical unit vectors. The KVU frames for $\mathrm{UAV}^{\mathrm{T}}$ and $\mathrm{UAV}^{\mathrm{H}}$ are denoted as t and h, respectively. The vectors $\hat{k}^{\mathrm{T}}$ and $\hat{k}^{\mathrm{H}}$ denote the DOA vector $\hat{k}$ as seen by the tracking and handoff UAVs in the global frame (Fig. 1). Since $\hat{k}^{\mathrm{T}}$ should equal $\hat{k}^{\mathrm{H}}$, we have the situation depicted in Fig. 2, where the two KVU frames are related by the simple rotation

$$\mathbf{M}_{\mathrm{h}}^{\mathrm{t}}(\alpha) = \begin{bmatrix} 1 & 0 & 0 \\ 0 & \cos\alpha & -\sin\alpha \\ 0 & \sin\alpha & \cos\alpha \end{bmatrix}, \tag{6}$$

where α is an unknown that cannot be deduced from DOA information alone. Conceptually, the $\hat{v}$-$\hat{u}$ axes in each frame are related by a single rotation angle α. Once α is known, the two UAV reference frames are related by

$$\mathbf{M}_{\mathrm{H}}^{\mathrm{T}}(\alpha) = \mathbf{M}_{\mathrm{H}}^{\mathrm{h}} \mathbf{M}_{\mathrm{h}}^{\mathrm{t}}(\alpha) \mathbf{M}_{\mathrm{t}}^{\mathrm{T}}. \tag{7}$$

The matrices $\mathbf{M}_{\mathrm{H}}^{\mathrm{h}}$ and $\mathbf{M}_{\mathrm{t}}^{\mathrm{T}}$ can be readily computed using (4) and (5) for $\mathrm{A} \in \{\mathrm{T}, \mathrm{H}\}$ and forming

$$\mathbf{M}_{\mathrm{t}}^{\mathrm{T}} = \left[\hat{k}_{\mathrm{T}}^{\mathrm{T}}\ \hat{v}_{\mathrm{T}}^{\mathrm{T}}\ \hat{u}_{\mathrm{T}}^{\mathrm{T}}\right]^{\dagger}, \tag{8}$$

$$\mathbf{M}_{\mathrm{H}}^{\mathrm{h}} = \left[\hat{k}_{\mathrm{H}}^{\mathrm{H}}\ \hat{v}_{\mathrm{H}}^{\mathrm{H}}\ \hat{u}_{\mathrm{H}}^{\mathrm{H}}\right], \tag{9}$$

which only requires local knowledge of $\hat{k}$.

B. Finding α Using the Polarimetric MIMO Channel

We now formulate a method for determining α by comparing measurements of the narrowband polarimetric MIMO channel between the two UAVs to a model of the channel. $\mathrm{UAV}^{\mathrm{T}}$ and $\mathrm{UAV}^{\mathrm{H}}$ have arrays with N_{T} and N_{H} antennas, respectively. It is most natural to define the field radiation pattern of each antenna element using the local frame aligned with that antenna. We therefore define Cartesian frames for the nth tracking and mth handoff antennas as $(\hat{x}_{\mathrm{T}}^{\mathrm{T}n}, \hat{y}_{\mathrm{T}}^{\mathrm{T}n}, \hat{z}_{\mathrm{T}}^{\mathrm{T}n})$ and $(\hat{x}_{\mathrm{H}}^{\mathrm{H}m}, \hat{y}_{\mathrm{H}}^{\mathrm{H}m}, \hat{z}_{\mathrm{H}}^{\mathrm{H}m})$, referred to as the $\mathrm{T}n$ and $\mathrm{H}m$ frames, respectively. Patterns are naturally defined in spherical KVU

frames given by $(\hat{k}_{\mathrm{T}n}^{\mathrm{T}n}, \hat{v}_{\mathrm{T}n}^{\mathrm{T}n}, \hat{u}_{\mathrm{T}n}^{\mathrm{T}n})$ and $(\hat{k}_{\mathrm{H}m}^{\mathrm{H}m}, \hat{v}_{\mathrm{H}m}^{\mathrm{H}m}, \hat{u}_{\mathrm{H}m}^{\mathrm{H}m})$, referred to as the $\mathrm{t}n$ and $\mathrm{h}m$ frames, respectively.

It is assumed that each antenna is simulated or measured in its local frame, such that the electric field patterns $\mathbf{e}_{\mathrm{t}n}^{\mathrm{T}n}(\hat{k}_{\mathrm{T}n}^{\mathrm{T}n})$ and $\mathbf{e}_{\mathrm{h}m}^{\mathrm{H}m}(\hat{k}_{\mathrm{H}m}^{\mathrm{H}m})$ are known. Note that for far-field patterns, the vector field expressed in the spherical basis is $[0\ e_\theta\ e_\phi]^\dagger$, since field polarized in the radiation direction is zero.

Modeling the channel between the two UAVs requires the pattern in the direction of $\hat{k}$ defined in each antenna frame, which is given by

$$\hat{k}_{\mathrm{T}n}^{\mathrm{T}n} = \mathbf{M}_{\mathrm{T}n}^{\mathrm{T}} \hat{k}_{\mathrm{T}}^{\mathrm{T}} \tag{10}$$

$$\hat{k}_{\mathrm{H}m}^{\mathrm{H}m} = -\mathbf{M}_{\mathrm{H}m}^{\mathrm{H}} \hat{k}_{\mathrm{H}}^{\mathrm{H}}, \tag{11}$$

where the minus sign ensures that $\hat{k}_{\mathrm{H}m}^{\mathrm{H}m}$ points radially away from $\mathrm{UAV}^{\mathrm{H}}$ for the definition of the handoff UAV antenna patterns. Note that the direction $\hat{k}$ in a KVU reference frame can be converted to spherical angles using

$$\phi = \tan^{-1}\left(k_y/k_x\right), \tag{12}$$

$$\theta = \tan^{-1}\left(\sqrt{k_x^2 + k_y^2}/k_z\right), \tag{13}$$

where (k_x, k_y, k_z) are the Cartesian components of $\hat{k}$, and ϕ and θ are the usual spherical azimuth and elevation angles.

With $\mathrm{UAV}^{\mathrm{T}}$ as the transmitter, the vector (polarized) field generated by the nth antenna in the reference frame for $\mathrm{UAV}^{\mathrm{H}}$ is given by

$$\mathbf{e}_{\mathrm{H}}^{\mathrm{T}n} = \mathbf{M}_{\mathrm{H}}^{\mathrm{T}}(\alpha)\mathbf{M}_{\mathrm{T}}^{\mathrm{T}n}\mathbf{M}_{\mathrm{T}n}^{\mathrm{t}n}\mathbf{e}_{\mathrm{t}n}^{\mathrm{T}n}. \tag{14}$$

With $\mathrm{UAV}^{\mathrm{H}}$ as the receiver, the polarized reception pattern of the mth antenna is

$$\mathbf{e}_{\mathrm{H}}^{\mathrm{H}m} = \mathbf{M}_{\mathrm{H}}^{\mathrm{H}m}\mathbf{M}_{\mathrm{H}m}^{\mathrm{h}m}\mathbf{e}_{\mathrm{h}m}^{\mathrm{H}m}. \tag{15}$$

With patterns in a common frame, we can compute the mnth entry of the channel transfer matrix $\mathbf{H}$ as

$$H_{mn}(\alpha) = (\mathbf{e}_{\mathrm{H}}^{\mathrm{T}n} \cdot \mathbf{e}_{\mathrm{H}}^{\mathrm{H}m}) \exp(j\psi_{mn}) \tag{16}$$

where ψ_{mn} is the RF phase shift from the nth tracking antenna to the mth handoff antenna, computed as

$$\psi_{\mathrm{mn}} = k_0(\mathbf{r}_{\mathrm{T}}^{\mathrm{T}n} \cdot \hat{k}_{\mathrm{T}}^{\mathrm{T}} - \mathbf{r}_{\mathrm{H}}^{\mathrm{H}m} \cdot \hat{k}_{\mathrm{H}}^{\mathrm{H}}), \tag{17}$$

$k_0 = 2\pi f/c$ is the wavenumber (for RF frequency f and speed of light c), and $\mathbf{r}_{\mathrm{T}}^{\mathrm{T}n}$ and $\mathbf{r}_{\mathrm{H}}^{\mathrm{H}m}$ are the position (assumed phase center) of the nth tracking and mth handoff antennas in their local UAV Cartesian frames, respectively.

We find α by searching for the value that gives the best fit between the measured MIMO channel $\mathbf{H}_{\mathrm{meas}}$ and the modeled value given in (16). We first stack the channels columnwise into column vectors, with the operation being denoted as

$$\mathbf{h}_{\mathrm{meas}} = \mathrm{Vec}\{\mathbf{H}_{\mathrm{meas}}\}, \tag{18}$$

$$\mathbf{h}(\alpha) = \mathrm{Vec}\{\mathbf{H}(\alpha)\}. \tag{19}$$

Since it is difficult to measure or estimate absolute amplitudes and phases of the channel matrix entries, we normalize the channel vectors according to

$$\underline{\mathbf{h}}_{\mathrm{meas}} = \mathbf{h}_{\mathrm{meas}}/h_{\mathrm{meas},\ell}, \tag{20}$$

$$\underline{\mathbf{h}}(\alpha) = \mathbf{h}(\alpha)/h_\ell(\alpha), \tag{21}$$

where $\ell = \arg\max_\ell |h_{\mathrm{meas},\ell}|$. Note that noise amplification due to this normalization should be small since the channel element with the maximum amplitude is always used. Finally, α is given by the solution of

$$\alpha_{\mathrm{opt}} = \arg\min_\alpha \|\underline{\mathbf{h}}_{\mathrm{meas}} - \underline{\mathbf{h}}(\alpha)\|^2. \tag{22}$$

Since we are only seeking a single real number over the interval $[-\pi, \pi)$ in (22), a simple one-dimensional parameter sweep can be used. The relation between the T and H frames can be found using (7), or

$$\mathbf{M}_{\mathrm{H}}^{\mathrm{T}}(\alpha_{\mathrm{opt}}) = [\hat{x}_{\mathrm{T}}^{\mathrm{H}}\ \hat{y}_{\mathrm{T}}^{\mathrm{H}}\ \hat{z}_{\mathrm{T}}^{\mathrm{H}}]^\dagger = [\hat{x}_{\mathrm{H}}^{\mathrm{T}}\ \hat{y}_{\mathrm{H}}^{\mathrm{T}}\ \hat{z}_{\mathrm{H}}^{\mathrm{T}}]. \tag{23}$$

Because absolute phase is unavailable, the phase normalization in (20) and (21) creates a 180° ambiguity in α, meaning $\mathbf{M}_{\mathrm{H}}^{\mathrm{T}}(\alpha_{\mathrm{opt}} + \pi)$ is also a candidate solution.

C. Resolving the 180° Ambiguity

Several methods for resolving the 180° ambiguity in α are described below.

1) Multiple Aspects: Appendix A proves that applying the method for two different values of $\hat{k}$ but for the same relative attitudes gives the same attitude estimates for the correct value of α but different attitude estimates for the solution $\alpha + \pi$. Removing the incorrect solution requires maneuvering to change the relative positions but not the relative attitudes of the UAVs. Linear motion is an example of such a maneuver. This technique is appropriate for UAVs that are close enough for the global $\hat{k}$ vector to change significantly (perhaps a few degrees) over a short time, which is not the case for widely separated UAVs.

2) Tracking: Given known initial relative attitudes, the method is applied often enough to allow comparison of subsequent attitude estimates. Using the correct value of α leads to correct attitude estimates that gradually change over time. Using the 180° ambiguity leads to a large jump in the attitude (typically 180°). In this way, as the relative pose is successively tracked, the α giving an attitude that is closest (such as in a least squared sense) to the previous step is retained as the correct solution. With the exception of obtaining the initial relative attitude estimate, it is expected that this technique could be used in virtually any scenario.

3) Attitude Constraints: For most UAVs, the range of attitudes that are consistent with controlled flight is limited. Often, the YPR associated with the solution $\alpha + \pi$ produces nonsensical attitudes, such as an overly steep roll or pitch angle or even a UAV flying upside down, allowing identification and rejection of the incorrect value of α. This kind of sanity checking should be used in conjunction with other methods, since not all ambiguities can be resolved this way.

4) Path-length Information: Methods such as those presented in [25], [27] use relative path distances between pairs of transmit and receive antennas to obtain unambiguous attitude estimates. Unfortunately, those methods require very high bandwidth to obtain high accuracy, especially at long range. However, if path-length methods are only used for resolving the 180° ambiguity, much less accuracy (and therefore bandwidth) is required. The basic strategy in our case would

be to estimate the path distances between a set of transmit (tracking) and receive (handoff) antennas. Given the two candidate estimates of α, two different attitudes are obtained. For each attitude, the relative path lengths can be computed and compared with the measured values, allowing the correct α to be identified. Although the ability of these methods to obtain an unambiguous estimate in a single snapshot is attractive, it is unclear how much RF bandwidth is needed. The development of such methods is left for future investigation.

5) Sensor Fusion: It is likely that most UAVs will not have to rely totally on RF resources for control and navigation, possibly incorporating an inertial measurement unit (IMU), magnetic compass, cameras, etc. Although outside the scope of this work, we expect that information from these sensors on the two UAVs could be combined to eliminate the 180° ambiguity, even when such sensors do not provide enough information for estimation of the three DOF relative attitude.

D. Algorithm

An algorithm applying the outlined method can be summarized as follows:

1) Estimate the $\mathrm{UAV}^{\mathrm{T}}$ DOA vector with a direction-finding technique [38] locally at $\mathrm{UAV}^{\mathrm{T}}$ and $\mathrm{UAV}^{\mathrm{H}}$ to obtain $\hat{k}_{\mathrm{T}}^{\mathrm{T}}$ and $\hat{k}_{\mathrm{H}}^{\mathrm{H}}$.
2) Use (4) and (5) to obtain $\hat{u}_{\mathrm{T}}^{\mathrm{T}}$, $\hat{v}_{\mathrm{T}}^{\mathrm{T}}$, $\hat{u}_{\mathrm{H}}^{\mathrm{H}}$, and $\hat{v}_{\mathrm{H}}^{\mathrm{H}}$ which give the local KVU frames for the two UAVs.
3) Form the transformation matrices $\mathbf{M}_{\mathrm{t}}^{\mathrm{T}}$ and $\mathbf{M}_{\mathrm{H}}^{\mathrm{h}}$ using (8) and (9).
4) Normalize the measured MIMO channel using (20).
5) Generate samples of α on the interval $[0, \pi]$, and for each candidate value of α perform the following steps:
   a) Compute $\mathbf{M}_{\mathrm{h}}^{\mathrm{t}}(\alpha)$ using (6).
   b) Compute $\mathbf{M}_{\mathrm{H}}^{\mathrm{T}}(\alpha)$ using (7).
   c) Compute the entries of the modeled MIMO channel by performing the following steps for all pairs of m and n:
      i) Construct $\mathbf{M}_{\mathrm{T}n}^{\mathrm{T}} = (\mathbf{M}_{\mathrm{T}}^{\mathrm{T}n})^{\dagger}$ and $\mathbf{M}_{\mathrm{H}m}^{\mathrm{H}} = (\mathbf{M}_{\mathrm{H}}^{\mathrm{H}m})^{\dagger}$ based on known orientations of the antennas relative to each local UAV frame.
      ii) Find $\hat{k}_{\mathrm{T}n}^{\mathrm{T}n}$ and $\hat{k}_{\mathrm{H}m}^{\mathrm{H}m}$ in the local antenna KVU frames of $\mathrm{UAV}^{\mathrm{T}}$ and $\mathrm{UAV}^{\mathrm{H}}$, respectively, using (10) and (11).
      iii) Look up the polarimetric patterns of the nth $\mathrm{UAV}^{\mathrm{T}}$ and mth $\mathrm{UAV}^{\mathrm{H}}$ antennas by converting the local $\hat{k}$ directions from the last step into spherical angles using (12) and (13). To allow a unique one-to-one mapping over the full $[-\pi, \pi)$ radian interval, $\tan^{-1}(a/b)$ should be computed using a 2-argument tangent function (hereafter designated as $\mathrm{atan2}(a, b)$).
      iv) Use (4) and (5) to form transformation matrices from each antenna's local spherical frame to its Cartesian frame:

$$\mathbf{M}_{\mathrm{T}n}^{\mathrm{t}n} = [\hat{k}_{\mathrm{T}n}^{\mathrm{T}n}\ \hat{u}_{\mathrm{T}n}^{\mathrm{T}n}\ \hat{v}_{\mathrm{T}n}^{\mathrm{T}n}], \tag{24}$$

$$\mathbf{M}_{\mathrm{H}m}^{\mathrm{h}m} = [\hat{k}_{\mathrm{H}m}^{\mathrm{H}m}\ \hat{u}_{\mathrm{H}m}^{\mathrm{H}m}\ \hat{v}_{\mathrm{H}m}^{\mathrm{H}m}]. \tag{25}$$

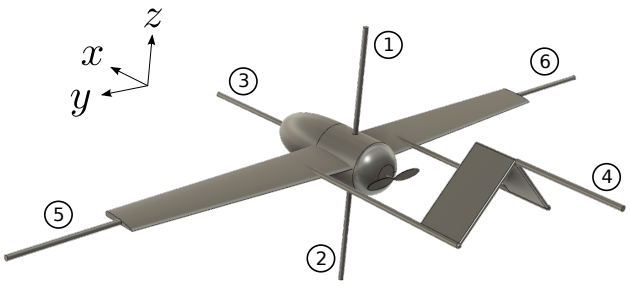

Fig. 3. UAV model simulated with FDTD. Numbered cylinders are six monopole antennas used for DOA and relative attitude estimation.

      v) Use (14) and (15) to transform the local polarimetric antenna patterns into a common frame of reference (the $\mathrm{UAV}^{\mathrm{H}}$ local frame).
      vi) Compute the channel matrix element with (16) and (17).
   d) Stack and normalize the estimated channel matrix obtained from the previous loop according to (21). Use the same normalization index as that used in the measured channel previously.
   e) Compare the modeled and measured MIMO channels according to (22).
6) Given the solution to (22) from the previous loop, referred to as α_{opt}, compute $\mathbf{M}_{\mathrm{H}}^{\mathrm{T}}$ using α_{opt} and $\alpha_{\mathrm{opt}} + \pi$, which are two candidate solutions giving the relative orientation vectors of the UAVs, as described in (23).
7) Use a method to resolve the 180° ambiguity (see Section III-C) and select the correct estimate of $\mathbf{M}_{\mathrm{H}}^{\mathrm{T}}$.

IV. Illustrative Numerical Examples

A. UAV Model and Antenna Configuration

A detailed UAV model was created using Autodesk Fusion360 as depicted in Fig. 3. The UAV has a wingspan of 1.5 m and nose-to-tail length of 0.8 m. Arguably, a high RF center frequency in the microwave or millimeter wave regime is ideal to reduce antenna size and weight. However, such high frequencies hamper the full-wave electromagnetic simulation of the complete UAV performed in this paper. Although we use a somewhat low center frequency of 200 MHz in this example, resulting in large antennas, practical implementations may use higher frequencies to minimize antenna size.

Although optimal antenna array design is beyond our present scope, we expect that accurate DOA estimation over the whole radiation sphere will require an antenna array with amplitude and/or phase variation with respect to DOA and no "dead spots" (directions where no antenna radiates effectively). Next, three-DOF relative attitude estimation requires detecting a rotation around the DOA vector, meaning that the MIMO channel must change due to these rotations. If usual unipolarized antennas are used, at least two antennas with distinct polarization need to be visible for each possible DOA.

Following the above observations, six quarter-wave monopole antennas were placed on the UAV as shown by the numbered cylinders in Fig. 3. Although each antenna only senses (or excites) a single polarization, three orthogonally

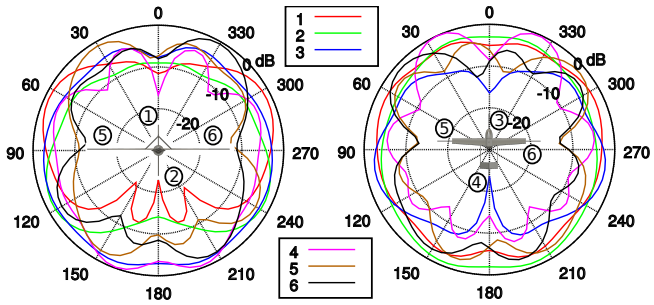

Fig. 4. Normalized antenna gain patterns (in dB) from FDTD simulations in the yz plane (left) and xy plane (right). Circled and boxed numbers indicate antenna indices. The small centered airplanes indicate the proper orientation of each plot relative to the UAV as well as the indexing of the antennas. Although 2D gain pattern cuts are plotted here, the algorithm uses complex polarimetric patterns over the full radiation sphere.

oriented antennas are visible for each DOA, allowing the full E-field polarization vector to be estimated for any DOA. Finite-difference time-domain (FDTD) simulations [39] were performed, where it was assumed that the UAV geometry is a perfect electrical conductor (PEC). Simulations were performed using a custom FDTD code that has been employed successfully in several previous modeling problems [40]. The FDTD simulation domain size was $3.0\ \mathrm{m} \times 3.6\ \mathrm{m} \times 2.4\ \mathrm{m}$ in the x, y, and z directions, respectively, and the FDTD unit cell size was 5 cm. Each antenna pattern was obtained by running a separate simulation with a gap voltage source placed across one of the antennas from the monopole base to the aircraft body and open-circuiting the other five antennas. Polarimetric far-field patterns were computed by integrating near fields on a box enclosing the complete UAV and using a standard near-to-far field transformation. Far fields were stored for the complete radiation sphere for each antenna with an angular resolution of 5° in both elevation and azimuth. This coarse sampling was chosen to show that attitude estimation is reliable even with non-ideal pattern knowledge.

Figure 4 plots normalized antenna gain patterns for all 6 antennas in the yz and xy planes. Although the antenna patterns do resemble monopoles with lower radiation along the monopole axis, the UAV body distorts the patterns.

B. DOA and Channel Estimation

This section describes how noisy DOA and MIMO channel estimates are obtained, which are used as inputs to the simulated attitude estimation algorithm.

1) Gaussian DOA Estimation Error: First, we focus on attitude estimation uninfluenced by algorithmic choices for the direction-finding method. The noisy estimate of the DOA vector is obtained by randomly rotating $\hat{k}$ using

$$\hat{k}_{\mathrm{est}} = \hat{k} \underbrace{\left[\hat{x}^{\mathrm{K}}\ \hat{y}^{\mathrm{K}}\ \hat{z}^{\mathrm{K}}\right]}_{\mathbf{M}_{\mathrm{K}}} \tag{26}$$

where the noise rotation matrix $\mathbf{M}_{\mathrm{K}}$ is constructed by generating zero-mean Gaussian random pitch, roll, and yaw angles, each with variance σ_{K}^2, and using the expressions in Appendix B to convert these vectors to an orientation matrix.

2) Table Lookup DOA Estimation: Existing beamforming and subspace methods [37], [38] may be used for DOA estimation, but these methods often require a special array structure or do not automatically handle multiple polarizations. To allow the same 6-element antenna array to be used for both MIMO channel and DOA estimation, a straightforward DOA estimation procedure based on a table lookup was developed and is described below. Drawbacks of this simple method include storage requirements for the database and a large number of required channel-table comparisons. Although the simple method meets our goal of illustrating correct performance of the attitude estimation algorithm, we hope that future work will adapt subspace-based methods to this problem, likely improving algorithmic efficiency and robustness.

Given the simulated antenna patterns, we can compute $\mathbf{h}_{\mathrm{exp}}(\theta, \phi, a, \nu)$, which represents the expected antenna array complex terminal voltages for local DOA direction (θ, ϕ) and incident polarization having axial ratio $|a|$ and tilt angle ν. Polarization handedness is specified by the sign of a where $a < 0$ ($a > 0$) indicates left (right) hand polarization.

A finite size table was computed by sampling

$$\theta = 0, 5^\circ, 10^\circ, \ldots, 180^\circ \tag{27}$$
$$\phi = 0, 5^\circ, 10^\circ, \ldots, 355^\circ \tag{28}$$
$$a = -1, -0.9, 0.8, \ldots, 0.9, 1 \tag{29}$$
$$\nu = 0, 5^\circ, 10^\circ, \ldots, 175^\circ, \tag{30}$$

which consists of $37 \times 73 \times 21 \times 36 = 2041956$ entries. Storage of the table requires 93 MB of memory for single precision floating point numbers assuming a 6-element array.

Once the table is computed, the local DOA vector at each UAV is estimated as follows. Assuming the tracking and handoff UAVs to be the transmitter and receiver, respectively, the handoff UAV finds the column of the channel $\mathbf{H}$ having the highest energy according to $\mathbf{h}_{\mathrm{max}}^{\mathrm{H}} = \mathbf{H}(:, n_0)$, where

$$n_0 = \arg\max_n \sum_m |H_{mn}|^2. \tag{31}$$

In practice, absolute amplitude and phase are difficult to recover, and the signal vector and table are normalized as

$$\underline{\mathbf{h}}_{\mathrm{max}}^{\mathrm{H}} = \mathbf{h}_{\mathrm{max}}^{\mathrm{H}} / h_{\mathrm{max},\ell}^{\mathrm{H}}, \tag{32}$$
$$\underline{\mathbf{h}}_{\mathrm{exp}} = \mathbf{h}_{\mathrm{exp}} / h_{\mathrm{exp},\ell}, \tag{33}$$

where $\ell = \arg\max_\ell |h_{\mathrm{max},\ell}^{\mathrm{H}}|$. Finally, the table is searched for the entry giving the least-square fit, or

$$(\theta^{\mathrm{H}}, \phi^{\mathrm{H}}, a^{\mathrm{H}}, \nu^{\mathrm{H}}) = \arg \min_{(\theta,\phi,a,\nu)} \|\underline{\mathbf{h}}_{\mathrm{max}}^{\mathrm{H}} - \underline{\mathbf{h}}_{\mathrm{exp}}(\theta, \phi, a, \nu)\|, \tag{34}$$

where θ^{H} and ϕ^{H} give the estimated elevation and azimuth angles of the local DOA vector at the handoff UAV. In an analogous way, the process is repeated on the row of $\mathbf{H}$ having the highest energy to obtain the local DOA vector at the tracking UAV, or θ^{T} and ϕ^{T}.

3) Channel Estimation Error: The exact MIMO channel estimates are corrupted using additive zero-mean complex Gaussian noise with variance

$$\sigma_{\mathrm{C}}^2 = 10^{-\mathrm{SNR_{dB}}/10} \max_{ij} |H_{ij}|^2, \tag{35}$$

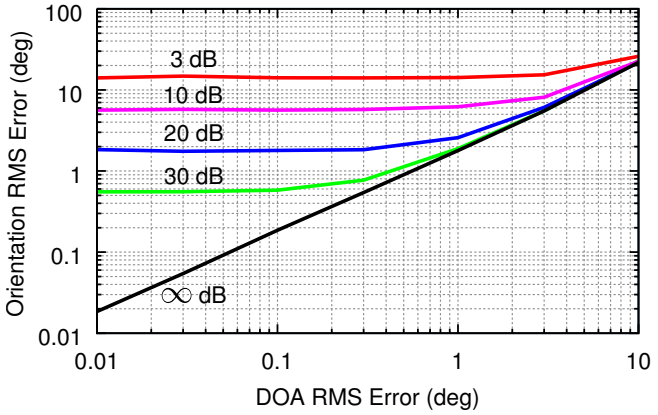

Fig. 5. RMS error of orientation vectors computed using 1000 random attitude realizations as a function of DOA RMS error, where each curve is for a fixed value of $\mathrm{SNR}_{\mathrm{dB}}$. The three orientation vectors have identical statistics, which were averaged.

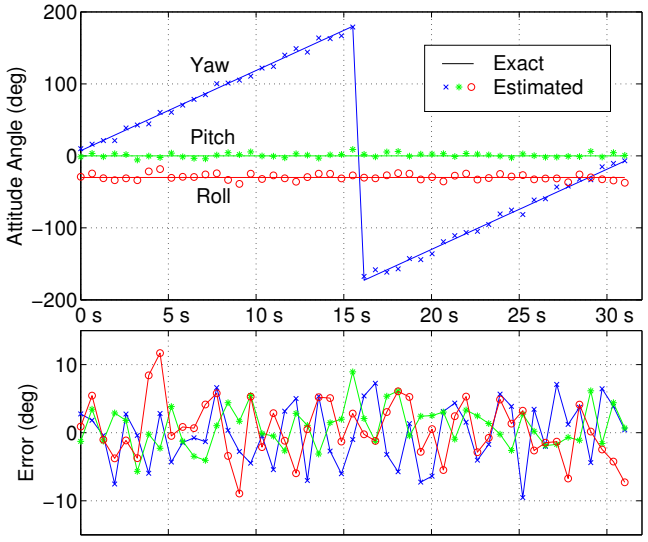

Fig. 6. Estimates of relative YPR versus time for one UAV flying in a circle of radius 150 m using a 30° bank around another fixed (hovering) UAV.

and $\mathrm{SNR}_{\mathrm{dB}}$ is the specified signal-to-noise ratio (SNR) in dB. Referencing the noise to the maximum channel gain removes the impact of antennas obstructed by the UAV that reduce the average gain and therefore essentially keeps the noise constant independent of relative UAV attitudes.

C. Performance vs. Estimation Error

To quantify the performance of the method with respect to error in the DOA and channel estimates, we implement the method for 1000 random orientations of the UAVs for different levels of estimation error. Simple Gaussian DOA estimation error is used, as described in Section IV-B1. The sphere of all possible attitudes is covered in these simulations by having yaw and roll uniform on $[0°, 360°]$ and pitch uniform on $[-90°, 90°]$. Given that we use random attitudes rather than practical flight maneuvers, we cannot apply the methods for ambiguity resolution of α, and therefore we simply choose the correct value of α based on the exact relative attitudes.

Using uniformly distributed random attitude angles can result in some extreme attitudes, and for some of these situations, slight errors in actual UAV orientation can lead to relatively large errors in YPR angles. Therefore, we directly quantify the angular error of the estimated orientation vectors $\hat{x}_{\mathrm{H}}^{\mathrm{T}}$, $\hat{y}_{\mathrm{H}}^{\mathrm{T}}$, and $\hat{z}_{\mathrm{H}}^{\mathrm{T}}$ using the expression

$$\epsilon_{\hat{r}} = \cos^{-1}(\hat{r}_{\mathrm{est}} \cdot \hat{r}_{\mathrm{exact}}), \tag{36}$$

where $\hat{r} \in \{\hat{x}_{\mathrm{H}}^{\mathrm{T}}, \hat{y}_{\mathrm{H}}^{\mathrm{T}}, \hat{z}_{\mathrm{H}}^{\mathrm{T}}\}$, and $(\cdot)_{\mathrm{est}}$ and $(\cdot)_{\mathrm{exact}}$ refer to estimated and exact quantities, respectively.

Fig. 5 shows the RMS error in the orientation vectors of the estimated UAV attitude as a function of the DOA estimation error. For infinite SNR, attitude estimation error is approximately double that of the DOA estimation error, resulting from the combination of independent DOA error at the tracking and handoff UAVs. For practical SNR, an error floor in the attitude estimate is experienced at low DOA error.

D. Single Circling UAV

In this example $\mathrm{UAV}^{\mathrm{T}}$ hovers in a fixed position at the origin while $\mathrm{UAV}^{\mathrm{H}}$ travels in a banked turn around $\mathrm{UAV}^{\mathrm{T}}$ at a constant radius. The free-space wavelength is $\lambda = 1.5$ m, the circling radius is 150 m, the speed is 100 km/h, the bank angle is 30°, and both UAVs are at the same altitude. Gaussian DOA error (Section IV-B1) of 3° is used, and SNR is 20 dB. In this case we resolve the ambiguity in α by rejecting relative pitch greater than 45° and relative roll greater than 90°. The results in Fig. 6 show that the attitude estimator is able to accurately determine the YPR angles, with RMS errors in these angles of $(4.4°, 3.1°, 4.3°)$.

E. Two Circling UAVs

Next we consider the case where *both* $\mathrm{UAV}^{\mathrm{T}}$ and $\mathrm{UAV}^{\mathrm{H}}$ fly in 30° banked turns (in opposite turn directions) on a circle of radius 150 m at 100 km/h with an altitude difference of 45 m. Due to the larger relative attitudes, we use multiple aspects (Section III-C1) to resolve the 180° ambiguity in α at the beginning of the maneuver and tracking thereafter. RMS DOA error and SNR are the same as the last example. Fig. 7 demonstrates that the method is able to accurately determine the YPR angles with respective RMS errors of $(4.4°, 4.4°, 4.1°)$.

F. Practical DOA Estimation

Finally, we explore the performance of a method that uses a practical DOA estimation method, illustrating that a single RF array can be used for both direction finding and attitude estimation. 1000 Monte Carlo simulations were performed with uniform random UAV attitude and DOA, similar to those in Section IV-C. Local DOA estimates were obtained using the table lookup method in Section IV-B2. Fig. 8 shows the cumulative distribution functions (CDFs) of the error for the local DOA estimates (solid curves), defined as

$$\epsilon_{\hat{k}} = \cos^{-1}(\hat{k}_{\mathrm{est}}^{\mathrm{H}} \cdot \hat{k}_{\mathrm{exact}}^{\mathrm{H}}). \tag{37}$$

Although DOA estimation performance is poor for 10 dB SNR, acceptable performance is obtained for 15 dB or higher,

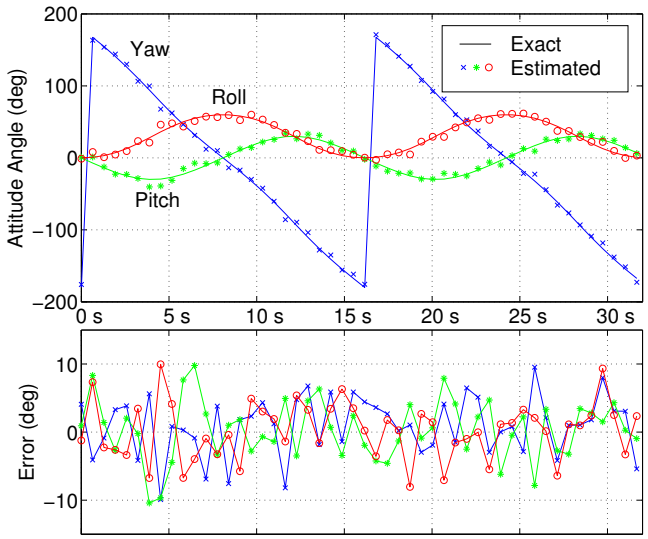

Fig. 7. Estimates of YPR versus time for two circling UAVs flying in 30° banked turns on circles of radius 150 m. The UAVs turn in opposite directions to provide constantly changing relative YPR.

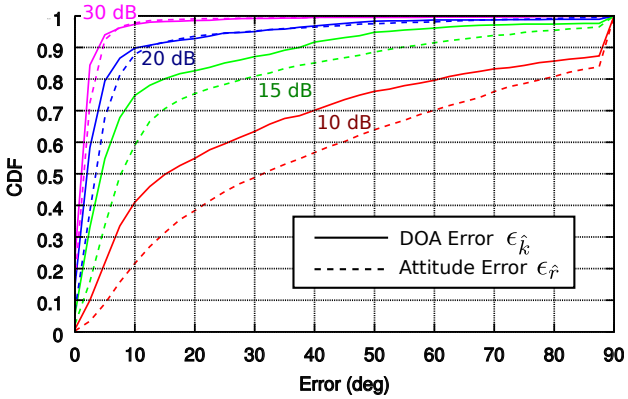

Fig. 8. Cumulative distribution functions (CDFs) of error for Monte Carlo simulations of attitude estimation using the table lookup method for local DOA estimation. Solid and dashed lines show error in local DOA estimates and resulting attitude estimates, respectively. Labels on the curves indicate the simulated receive SNR.

where 10° of error or better is obtained with probability 0.75, 0.9, and 0.97, for 15, 20, and 30 dB SNR, respectively. Fig. 8 also shows the error of the resulting attitude estimates (dashed curves). For low to moderate SNR, relatively high error in the DOA estimates leads to even higher error in the attitude estimation. However, for high SNR, error in the attitude estimate becomes similar to that of the DOA estimates, approaching a bound of about 5°, which is the resolution of the pattern lookup table. In practice, 5° of error in relative attitude may not be sufficient for some applications, suggesting that interpolation or more detailed patterns should be used.

A troubling aspect of Fig. 8 is the heavy-tail behavior that could lead to poor performance with a tracking filter. The heavy tails in the error distributions are due to infrequent cases where the DOA vector at one of the UAVs has large error, leading to very high error in the resulting attitude estimate. Fortunately, these cases can usually be detected by checking the fidelity of the fit between the estimated and modeled

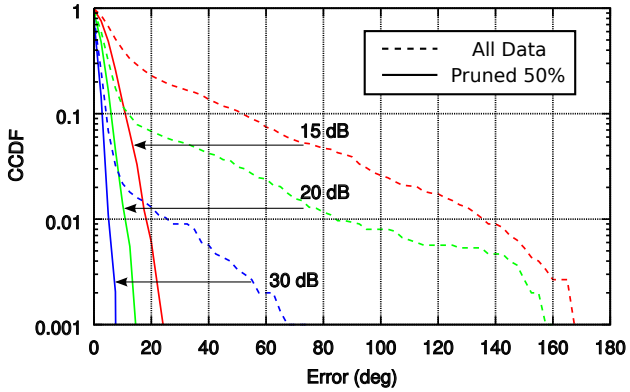

Fig. 9. Complementary cumulative distribution functions (CCDFs) from Monte Carlo simulations of the original table-lookup algorithm (Fig. 8) indicated by "All Data," and a modified algorithm where 50% of the estimates are discarded ("Pruned 50%") according to ϵ_H. Significant reduction of the error tails is obtained.

MIMO channel, or $\epsilon_H = \|\underline{\mathbf{h}}_{\text{meas}} - \underline{\mathbf{h}}(\alpha_{\text{opt}})\|^2$. If ϵ_H is much larger than typical values, this usually indicates a poor attitude estimate. Fig. 9 explores an improved algorithm that discards attitude estimates having ϵ_H greater than the median. Statistics of ϵ_H can be obtained through simulation or collected during system operation. Fig. 9 plots the complimentary CDF (CCDF) of attitude estimation error for three SNR levels for the original and improved algorithm, indicating that far more robust estimates (shorter tails) are obtained.

V. Conclusion

This paper presents a method for finding the relative attitude of two UAVs using only radio direction finding and MIMO channel estimation techniques. The method is useful in situations where GPS access and/or precise attitude information from gyros/accelerometers is not available. The problem solution uses the DOA vector to estimate two degrees of freedom, reducing the unknown relative attitude to a single angle α that is then estimated using observation of the polarimetric MIMO channel. Since the narrowband, polarimetric, far-field MIMO channel only gives enough information to resolve α to within a 180° ambiguity, several methods based on practical considerations or controlled maneuvers are provided for ambiguity resolution.

Simulations based on the proposed algorithm for realistic system parameters and flight profiles show that the method is able to estimate all three DOFs of UAV relative attitude. Monte Carlo simulations based on random UAV attitudes demonstrate that error in the orientation vectors is proportional to both the error in the DOA vector estimate as well as the SNR of the channel estimate.

Appendix

A. *Proof of Shifting $\hat{k}$ Method*

The purpose of this appendix is to prove that the 180° ambiguity in α can always be resolved by keeping the aircraft attitudes constant while changing $\hat{k}$ by a small amount.

Consider an arbitrary vector $\mathbf{r}_{\text{T}}$ in the tracking frame. The handoff UAV estimates the same vector in the handoff frame

for two DOA vectors $\hat{k}^{(1)}$ and $\hat{k}^{(2)}$ with $\hat{k}^{(1)} \neq \hat{k}^{(2)}$, resulting in estimates $\mathbf{r}_{\mathrm{H}}^{(1)}$ and $\mathbf{r}_{\mathrm{H}}^{(2)}$ when the correct α is used and $\mathbf{r}_{\mathrm{H}}^{(1)\prime}$ and $\mathbf{r}_{\mathrm{H}}^{(2)\prime}$ when $\alpha+\pi$ is used. Recall that the correct α aligns $\hat{u}^{\mathrm{T}}$ and $\hat{v}^{\mathrm{T}}$ with $\hat{u}^{\mathrm{H}}$ and $\hat{v}^{\mathrm{H}}$ in any common reference frame (see Fig. 2). But when $\alpha+\pi$ is selected, we have

$$\mathbf{M}_{\mathrm{h}}^{\mathrm{t}}(\alpha+\pi) = \mathbf{M}_{\mathrm{h}}^{\mathrm{t}}(\alpha) \underbrace{\begin{bmatrix} 1 & 0 & 0 \\ 0 & -1 & 0 \\ 0 & 0 & -1 \end{bmatrix}}_{\mathbf{L}}. \tag{38}$$

This means that

$$\mathbf{r}_{\mathrm{H}}^{(\ell)} = \mathbf{M}_{\mathrm{H}}^{\mathrm{h}(\ell)}\mathbf{M}_{\mathrm{h}}^{\mathrm{t}(\ell)}\mathbf{M}_{\mathrm{t}}^{\mathrm{T}(\ell)}\mathbf{r}_{\mathrm{T}} \tag{39}$$

$$\mathbf{r}_{\mathrm{H}}^{(\ell)\prime} = \mathbf{M}_{\mathrm{H}}^{\mathrm{h}(\ell)}\mathbf{L}\mathbf{M}_{\mathrm{h}}^{\mathrm{t}(\ell)}\mathbf{M}_{\mathrm{t}}^{\mathrm{T}(\ell)}\mathbf{r}_{\mathrm{T}}, \tag{40}$$

where $\ell \in 1,2$ for the two different cases of $\hat{k}$ and the dependence on α is dropped in the notation since all quantities now assume the correct value of α. In the absence of noise and estimation error, by construction our algorithm always gives the correct estimate of $\mathbf{r}_{\mathrm{H}}$ regardless of $\hat{k}$ when α is correct, meaning $\mathbf{r}_{\mathrm{H}}^{(1)} = \mathbf{r}_{\mathrm{H}}^{(2)}$, which implies

$$\mathbf{M}_{\mathrm{H}}^{\mathrm{h}(1)}\mathbf{M}_{\mathrm{h}}^{\mathrm{t}(1)}\mathbf{M}_{\mathrm{t}}^{\mathrm{T}(1)}\mathbf{r}_{\mathrm{T}} = \mathbf{M}_{\mathrm{H}}^{\mathrm{h}(2)}\mathbf{M}_{\mathrm{h}}^{\mathrm{t}(2)}\mathbf{M}_{\mathrm{t}}^{\mathrm{T}(2)}\mathbf{r}_{\mathrm{T}}. \tag{41}$$

In contrast, when $\alpha+\pi$ is selected, we have

$$\mathbf{r}_{\mathrm{H}}^{(1)\prime} = \mathbf{M}_{\mathrm{H}}^{\mathrm{h}(1)}\mathbf{L}\mathbf{M}_{\mathrm{h}}^{\mathrm{t}(1)}\mathbf{M}_{\mathrm{t}}^{\mathrm{T}(1)}\mathbf{r}_{\mathrm{T}} \tag{42}$$

$$= \mathbf{M}_{\mathrm{H}}^{\mathrm{h}(1)}\mathbf{L}\mathbf{M}_{\mathrm{h}}^{\mathrm{H}(1)}\mathbf{M}_{\mathrm{H}}^{\mathrm{h}(2)}\mathbf{M}_{\mathrm{h}}^{\mathrm{t}(2)}\mathbf{M}_{\mathrm{t}}^{\mathrm{T}(2)}\mathbf{r}_{\mathrm{T}}, \tag{43}$$

where the second equality comes from using (41) with $(\mathbf{M}_{\mathrm{H}}^{\mathrm{h}(1)})^{-1} = \mathbf{M}_{\mathrm{h}}^{\mathrm{H}(1)}$. Next, from (40) and (43) we compute the difference of the two estimates as

$$\mathbf{r}_{\mathrm{H}}^{(2)\prime} - \mathbf{r}_{\mathrm{H}}^{(1)\prime} = \underbrace{(\mathbf{M}_{\mathrm{H}}^{\mathrm{h}(2)}\mathbf{L} - \mathbf{M}_{\mathrm{H}}^{\mathrm{h}(1)}\mathbf{L}\mathbf{M}_{\mathrm{h}}^{\mathrm{H}(1)}\mathbf{M}_{\mathrm{H}}^{\mathrm{h}(2)})}_{\mathbf{Q}}\mathbf{M}_{\mathrm{h}}^{\mathrm{t}(2)}\mathbf{M}_{\mathrm{t}}^{\mathrm{T}(2)}\mathbf{r}_{\mathrm{T}}. \tag{44}$$

Since the basis transformation matrices are always full rank, the only way this difference can be zero for all vectors $\mathbf{r}_{\mathrm{T}}$ is for $\mathbf{Q}$ to be the zero matrix. This requires

$$\mathbf{M}_{\mathrm{H}}^{\mathrm{h}(2)}\mathbf{L}\mathbf{M}_{\mathrm{h}}^{\mathrm{H}(2)} = \mathbf{M}_{\mathrm{H}}^{\mathrm{h}(1)}\mathbf{L}\mathbf{M}_{\mathrm{h}}^{\mathrm{H}(1)}. \tag{45}$$

Using (8), (9) and $\mathbf{L}$ from (38), we can express (45) as

$$\hat{k}_{\mathrm{H}}^{\mathrm{H}(1)}(\hat{k}_{\mathrm{H}}^{\mathrm{H}(1)})^{\dagger} - [\hat{v}_{\mathrm{H}}^{\mathrm{H}(1)}(\hat{v}_{\mathrm{H}}^{\mathrm{H}(1)})^{\dagger} + \hat{u}_{\mathrm{H}}^{\mathrm{H}(1)}(\hat{u}_{\mathrm{H}}^{\mathrm{H}(1)})^{\dagger}] = \hat{k}_{\mathrm{H}}^{\mathrm{H}(2)}(\hat{k}_{\mathrm{H}}^{\mathrm{H}(2)})^{\dagger} - [\hat{v}_{\mathrm{H}}^{\mathrm{H}(2)}(\hat{v}_{\mathrm{H}}^{\mathrm{H}(2)})^{\dagger} + \hat{u}_{\mathrm{H}}^{\mathrm{H}(2)}(\hat{u}_{\mathrm{H}}^{\mathrm{H}(2)})^{\dagger}]. \tag{46}$$

We know from properties of basis transformations that $\mathbf{M}_{\mathrm{H}}^{\mathrm{h}(\ell)}\mathbf{M}_{\mathrm{h}}^{\mathrm{H}(\ell)} = \mathbf{I}$, where $\mathbf{I}$ is the identity matrix, or

$$\hat{k}_{\mathrm{H}}^{\mathrm{H}(\ell)}(\hat{k}_{\mathrm{H}}^{\mathrm{H}(\ell)})^{\dagger} + \hat{v}_{\mathrm{H}}^{\mathrm{H}(\ell)}(\hat{v}_{\mathrm{H}}^{\mathrm{H}(\ell)})^{\dagger} + \hat{u}_{\mathrm{H}}^{\mathrm{H}(\ell)}(\hat{u}_{\mathrm{H}}^{\mathrm{H}(\ell)})^{\dagger} = \mathbf{I}, \tag{47}$$

which simplifies (46) to

$$\hat{k}_{\mathrm{H}}^{\mathrm{H}(1)}(\hat{k}_{\mathrm{H}}^{\mathrm{H}(1)})^{\dagger} = \hat{k}_{\mathrm{H}}^{\mathrm{H}(2)}(\hat{k}_{\mathrm{H}}^{\mathrm{H}(2)})^{\dagger}. \tag{48}$$

The only way for these outer products to be equal is for $\hat{k}_{\mathrm{H}}^{\mathrm{H}(1)} = \pm\hat{k}_{\mathrm{H}}^{\mathrm{H}(2)}$, but this either contradicts our initial assumption or requires a large maneuver that exchanges the relative location of the two UAVs. Precluding the latter case, we must have $\mathbf{Q} \neq 0$.

The meaning of this result is that if the incorrect value of α is used, there exist some vectors $\mathbf{r}_{\mathrm{T}}$ that will be estimated differently as $\hat{k}$ changes, even though the relative UAV attitudes remain constant. However, when the correct value of α is used, the same estimate will be obtained independent of $\hat{k}$. A convenient set of test vectors for $\mathbf{r}_{\mathrm{T}}$ is $(\hat{x}_{\mathrm{T}}^{\mathrm{T}}, \hat{y}_{\mathrm{T}}^{\mathrm{T}}, \hat{z}_{\mathrm{T}}^{\mathrm{T}})$, since the algorithm in this paper already estimates those in the handoff frame as $(\hat{x}_{\mathrm{H}}^{\mathrm{T}}, \hat{y}_{\mathrm{H}}^{\mathrm{T}}, \hat{z}_{\mathrm{H}}^{\mathrm{T}})$ or $\mathbf{M}_{\mathrm{H}}^{\mathrm{T}}$. Note that it is possible for (44) to be zero for some test vectors, but since $\mathbf{M}_{\mathrm{h}}^{\mathrm{t}(2)}\mathbf{M}_{\mathrm{t}}^{\mathrm{T}(2)}$ in (44) is full rank, the error cannot be zero for all three orthogonal vectors $(\hat{x}_{\mathrm{T}}^{\mathrm{T}}, \hat{y}_{\mathrm{T}}^{\mathrm{T}}, \hat{z}_{\mathrm{T}}^{\mathrm{T}})$ when the incorrect α is used.

B. Relation of Orientation Frames to Euler Angles

This paper employs frames rather than Euler angles of rotation, since this approach simplifies the analysis and does not suffer from ambiguities due to order of rotation. However, it may be desirable to convert from a frame to Euler angles and vice versa, and this appendix provides such expressions. For this purpose we assume the YPR (yaw, pitch, roll) order of rotations, which is usually standard in aviation. Yaw (Y), pitch (P), and roll (R) angles are defined as rotation about the $\hat{z}^{\mathrm{T}}$, $\hat{y}^{\mathrm{T}}$, and $\hat{x}^{\mathrm{T}}$ axes, respectively (Fig. 1), with the positive direction given by the right hand rule.

1) YPR to Orientation: Yaw (Y) and pitch (P) define the direction of the $\hat{x}^{\mathrm{T}}$ vector, analogous to how ϕ and θ define the direction of the $\hat{r}$ vector in spherical coordinates, or

$$\hat{x}^{\mathrm{T}} = [\cos(P)\cos(Y) \quad \cos(P)\sin(Y) \quad -\sin(P)]^{\dagger} \tag{49}$$

The other vectors for the case of *zero roll* can be found as

$$\underline{\hat{y}}^{\mathrm{T}} = (\hat{z} \times \hat{x}^{\mathrm{T}})/\|\hat{z} \times \hat{x}^{\mathrm{T}}\| \tag{50}$$

$$\underline{\hat{z}}^{\mathrm{T}} = \hat{x}^{\mathrm{T}} \times \underline{\hat{y}}^{\mathrm{T}}/\|\hat{x}^{\mathrm{T}} \times \underline{\hat{y}}^{\mathrm{T}}\|, \tag{51}$$

where $\hat{z} = [0\ 0\ 1]^{\dagger}$. Finally, roll (R) can be applied to obtain

$$\hat{y}^{\mathrm{T}} = \underline{\hat{y}}^{\mathrm{T}}\cos(R) + \underline{\hat{z}}^{\mathrm{T}}\sin(R) \tag{52}$$

$$\hat{z}^{\mathrm{T}} = -\underline{\hat{y}}^{\mathrm{T}}\sin(R) + \underline{\hat{z}}^{\mathrm{T}}\cos(R) \tag{53}$$

2) Orientation to YPR: Again, direction of the nose $(\hat{x}^{\mathrm{T}})$ gives pitch and yaw like in spherical coordinates, or

$$Y = \mathrm{atan2}(\hat{x}_2^{\mathrm{T}}, \hat{x}_1^{\mathrm{T}}) \tag{54}$$

$$P = -\mathrm{atan2}\left(\hat{x}_3^{\mathrm{T}}, \sqrt{(\hat{x}_1^{\mathrm{T}})^2 + (\hat{x}_2^{\mathrm{T}})^2}\right), \tag{55}$$

where $\hat{x}_i^{\mathrm{T}}$ denotes the ith element of the unit vector. The zero roll vectors $\underline{\hat{y}}^{\mathrm{T}}$ and $\underline{\hat{z}}^{\mathrm{T}}$ are found according to (50) and (51), and roll can then be computed as

$$R = \mathrm{atan2}(\hat{y}^{\mathrm{T}} \cdot \underline{\hat{z}}^{\mathrm{T}}, \hat{y}^{\mathrm{T}} \cdot \underline{\hat{y}}^{\mathrm{T}}). \tag{56}$$

REFERENCES

[1] W. F. Phillips, C. E. Hailey, and G. A. Gebert, "Review of attitude representations used for aircraft kinematics," *J. Aircraft*, vol. 38, pp. pp. 718–737, Jul./Aug. 2001.

[2] A. C. Sanderson, "A distributed algorithm for cooperative navigation among multiple mobile robots," *Advanced Robotics*, vol. 12, pp. 335–349, 1997.

[3] S. I. Roumeliotis and G. A. Bekey, "Distributed multirobot localization," *IEEE Trans. Robotics and Automation*, vol. 18, pp. 781–795, Oct. 2002.

[4] V. Indelman, P. Gurfil, E. Rivlin, and H. Rotstein, "Graph-based distributed cooperative navigation," in *Proc. 2011 IEEE Intl. Conf. Robotics and Automation*, Shanghai, China, May 9-13, 2011, pp. 4786–4791.
[5] R. Sharma, S. Quebe, R. W. Beard, and C. N. Taylor, "Bearing-only cooperative localization." *J. Intelligent and Robotic Systems*, vol. 72, pp. 429–440, Dec. 2013.
[6] S. Chung, A. A. Paranjape, P. Dames, S. Shen, and V. Kumar, "A survey on aerial swarm robotics," *IEEE Trans. Robotics*, vol. 34, no. 4, pp. 837–855, Aug 2018.
[7] P. Groves, *Principles of GNSS Inertial and Multisensor Integrated Navigation Systems*. Artech House, 2007.
[8] O. Woodman, "An introduction to inertial navigation," University of Cambridge, Tech. Rep. UCAMCL-TR-696, 2007.
[9] D. Biezad, *Integrated Navigation and Guidance Systems*, ser. AIAA Education Series. American Institute of Aeronautics and Astronautics, 1999.
[10] S. M. Ettinger, M. C. Nechyba, P. G. Ifju, and M. Waszak, "Vision-guided flight stability and control for micro air vehicles," in *Proc. 2002 IEEE/RSJ Intl. Conf. Intelligent Robots and Systems*, vol. 3, Lausanne, Switzerland, Sep. 30 - Oct. 4, 2002, pp. 2134–2140.
[11] D. Dusha, L. Mejias, and R. Walker, "Fixed-wing attitude estimation using tempoaral tracking of the horizon and optical flow," *J. Field Robotics*, vol. 28, pp. 355–372, Mar. 2011.
[12] D. Dusha, "Integrated vision-based attitude estimation," Ph.D. dissertation, Queensland University of Technology, 2012.
[13] A. E. R. Shabayek, C. Demonceaux, O. Morel, and D. Fofi, "Vision based UAV attitude estimation: Progress and insights," *J. Intelligent and Robotic Systems*, vol. 65, pp. 295–308, Jan. 2012.
[14] M. H. Tehrani, M. A. Garratt, and S. G. Anavatti, "Low-altitude horizon-based aircraft attitude estimation using UV-filtered panoramic images and optic flow," *IEEE Trans. Aerospace and Electronic Systems*, vol. 52, no. 5, pp. 2362–2375, Oct. 2016.
[15] G. Lu, M. E. Cannon, G. Lachapelle, and P. Kielland, "Attitude determination using dedicated and nondedicated multiantenna GPS sensors," *IEEE Trans. Aerospace and Electronic Systems*, vol. 30, pp. 1053–1058, Oct. 1994.
[16] H. M. Peng, E. R. Chang, and L. S. Wang, "Rotation method for direction finding via GPS carrier phases," *IEEE Trans. Aerospace and Electronic Systems*, vol. 36, no. 1, pp. 72–84, Jan. 2000.
[17] L. Lau, P. Cross, and M. Steen, "Flight tests of error-bounded heading and pitch determination with two GPS receivers," *IEEE Trans. Aerospace and Electronic Systems*, vol. 48, no. 1, pp. 388–404, Jan 2012.
[18] P. Henkel and M. Iafrancesco, "Tightly coupled position and attitude determination with two low-cost GNSS receivers," in *Proc. 11th Intl. Symp. Wireless Communications Systems (ISWCS)*, Barcelona, Spain, Aug. 26-29, 2014, pp. 895–900.
[19] J. N. Gross, Y. Gu, M. B. Rhudy, S. Gururajan, and M. R. Napolitano, "Flight-test evaluation of sensor fusion algorithms for attitude estimation," *IEEE Trans. Aerospace and Electronic Systems*, vol. 48, no. 3, pp. 2128–2139, July 2012.
[20] Z. Wu, M. Yao, H. Ma, W. Jia, and F. Tian, "Low-cost antenna attitude estimation by fusing inertial sensing and two-antenna GPS for vehicle-mounted satcom-on-the-move," *IEEE Trans. Veh. Technol.*, vol. 62, pp. 1084–1096, March 2013.
[21] H. Bai and R. W. Beard, "Relative heading estimation and its application in target handoff in GPS-denied environments," *IEEE Trans. Control Systems Technology*, vol. 27, no. 1, pp. 74–85, Jan. 2019.
[22] S. T. G. Maguire and P. A. Robertson, "Low frequency radio polarization sensor with applications in attitude estimation," *IEEE Sensors J.*, vol. 15, pp. 7304–7311, Dec. 2015.
[23] ——, "UAV attitude estimation using low-frequency radio polarization measurements," *IEEE Trans. Aerospace and Electronic Systems*, vol. 53, pp. 2–11, Feb. 2017.
[24] S. D. Silverstein, J. M. Ashe, G. M. Kautz, F. W. Wheeler, and A. Jacomb-Hood, "Tripulse: A system for determining orientation and attitude of a satellite borne active phased array," *IEEE Trans. Aerospace and Electronic Systems*, vol. 38, pp. 2–12, Jan. 2002.
[25] M. A. M. Marinho, R. S. J. Ferreira, J. P. C. L. d. Costa, E. P. d. Freitas, F. Antreich, K. Liu, H. C. So, R. T. d. J. Sousa, and R. Zelenovsky, "Antenna array based positioning scheme for unmanned aerial vehicles," in *Proc. 2013 ITG Workshop Smart Antennas*, Stuttgart, Germany, Mar. 13-14, 2013.
[26] J. S. Knogl, P. Henkel, and C. Günther, "Attitude estimation based on multibeam antenna signal power levels," in *Proc. 2013 ELMAR Symp.*, Zadar, Croatia, Sep. 25-27, 2013, pp. 341–344.
[27] M. Weiqing, R. Liu, Y. Xinxin, and E. Kamel, "Analysis of precision estimation of RF metrology in satellite formation flying," in *Proc. 2015 Intl. Conf. Wireless Communications Signal Processing (WCSP)*, Nanjing, China, Oct. 15-17 2015, pp. 1–5.
[28] J. P. C. L. da Costa, S. Schwarz, and L. F. de A. Gadêlha, "Attitude determination for unmanned aerial vehicles via an antenna array," in *Proc. 2012 ITG Workshop Smart Antennas*, Dresden, Germany, Mar. 7-8, 2012, pp. 264–268.
[29] T. F. K. Cordeiro, J. P. L. da Costa, K. Liu, and G. A. Borges, "Kalman-based attitude estimation for an UAV via an antenna array," in *Proc. 2014 Intl. Conf. Signal Processing and Commun. Systems (ICSPCS)*, Gold Coast, Australia, Dec. 15-17, 2014.
[30] X. Wang, X. Shao, D. Gong, and D. Duan, "Radio/VISNAV integrated navigation system for autonomous spacecraft rendezvous using two-order filter," in *Proc. 8th World Congress on Intelligent Control and Automation*, Jinan, China, July 7-9, 2010, pp. 1735–1740.
[31] G. A. Narciandi, J. Laviada, and F. Las-Heras, "Object attitude estimation using passive RFID tag arrays," in *Proc. 2016 URSI Intl. Symp. Electromagnetic Theory (EMTS)*, Espoo, Finland, Aug. 14-16, 2016, pp. 572–574.
[32] J. Hardy, J. Strader, J. N. Gross, Y. Gu, M. Keck, J. Douglas, and C. N. Taylor, "Unmanned aerial vehicle relative navigation in GPS denied environments," in *IEEE/ION Position, Location and Navigation Symposium (PLANS)*, Savannah, GA, Apr. 11-14, 2016, pp. 344–352.
[33] R. Sharma and C. Taylor, "Cooperative navigation of MAVs in GPS denied areas," in *Proc. 2008 Intl. Conf. Multisensor Fusion and Integration for Intelligent Systems*, Seoul, South Korea, Aug. 20-22, 2008, pp. 481–486.
[34] A. Mahmood, J. W. Wallace, and M. A. Jensen, "Radio frequency UAV attitude estimation using direction of arrival and polarization," in *Proc. 2017 European Conf. Antennas and Propag.*, Paris, France, Mar. 19-24, 2017, pp. 1857–1859.
[35] ——, "UAV attitude estimation using antenna arrays," in *Proc. 2017 IEEE Antennas and Propag. Society Intl. Symp.*, San Diego, USA, July 9-14, 2017, pp. 1863–1864.
[36] P. H. Zipfel, "Frames and coordinate systems," in *Modeling and simulation of aerospace vehicle dynamics*. Reston, VA: AIAA, 2007.
[37] L. C. Godara, "Application of antenna arrays to mobile communications. II. Beam-forming and direction-of-arrival considerations," *Proc. IEEE*, vol. 85, pp. 1195–1245, Aug. 1997.
[38] H. Krim and M. Viberg, "Two decades of array signal processing research: The parametric approach," *IEEE Signal Processing Magazine*, vol. 13, pp. 67–94, Jul. 1996.
[39] A. Taflove and S. C. Hagness, *Computational Electrodynamics: The Finite Difference Time Domain Method*. Artech House, 2000.
[40] J. W. Wallace, "Modeling electromagnetic wave propagation in electrically large structures," Ph.D. dissertation, Brigham Young University, 2002.

Jon W. Wallace (S'99-M'03-SM'13) received the B.S. (summa cum laude) and Ph.D. degrees in electrical engineering from Brigham Young University, Provo, UT, USA, in 1997 and 2002, respectively.

He was with Jacobs University, Bremen, Germany, from 2006 to 2013, and Wavetronix, LLC, Provo, UT, USA, from 2013 to 2014. Since 2014, he has been with the Department of Electrical and Computer Engineering, Lafayette College, Easton, PA, USA. His current research interests include physical layer security, MIMO communications and radar, and unmanned aircraft systems.

Dr. Wallace was a recipient of the National Science Foundation Graduate Fellowship in 1998. In 2002, he received the Harold A. Wheeler Applications Prize Paper Award in IEEE TRANSACTIONS ON ANTENNAS AND PROPAGATION. He has served as an Associate Editor of IEEE TRANSACTIONS ON ANTENNAS AND PROPAGATION, IEEE TRANSACTIONS ON WIRELESS COMMUNICATIONS, and IEEE TRANSACTIONS ON AEROSPACE AND ELECTRONIC SYSTEMS.

Attiya Mahmood (S'13-M'19) received the B.Sc. degree in computer engineering from the University of Engineering and Technology, Taxila, Pakistan in 2007, the M.Sc. degree in computer engineering from National University of Science and Technology, Rawalpindi, Pakistan in 2009, and the Ph.D. degree in electrical and computer engineering from Brigham Young University (BYU), Provo, UT, USA in 2018. From 2009 to 2011 she worked as a Lecturer at Institute of Space Technology, Pakistan and later joined Jacobs University, Germany as a research associate until January 2013. She is currently working as a Research Engineer at Wavetronix LLC, Provo, UT, USA. Her research interests include physical layer security, radars, MIMO communications, and array signal processing.

Michael A. Jensen (S'93-M'95-SM'01-F'08) received the B.S. and M.S. degrees from Brigham Young University (BYU), Provo, UT, in 1990 and 1991, respectively, and the Ph.D. degree from the University of California, Los Angeles, in 1994, all in electrical engineering. Since 1994, he has been at the Electrical and Computer Engineering Department, BYU, where he is currently a University Professor and Dean of the Ira A. Fulton College of Engineering. His research interests include antennas and propagation for communications, microwave circuit design, multi-antenna signal processing, and physical layer security.

Dr. Jensen is Past President of the IEEE Antennas and Propagation Society. He was previously the Editor-in-Chief of the IEEE TRANSACTIONS ON ANTENNAS AND PROPAGATION as well as an Associate Editor for the same journal and for the IEEE ANTENNAS AND WIRELESS PROPAGATION LETTERS. He has been a member and Chair of the Joint Meetings Committee for the IEEE Antennas and Propagation Society, a member of the society AdCom, a member of the society Publications Committee, and Co-Chair or Technical Program Chair for six society-sponsored symposia. In 2002, he received the Harold A. Wheeler Applications Prize Paper Award in the IEEE TRANSACTIONS ON ANTENNAS AND PROPAGATION. He was elevated to the grade of IEEE Fellow in 2008 in recognition of his research on multi-antenna communication.

Rashid Mehmood (S'05-M'16) received the B.Sc. (cum laude) degree in Communication Systems Engineering from the Institute of Space Technology (IST) in Pakistan in 2007, and the M.Sc. in Electrical Engineering from Jacobs University Bremen (JUB) in Germany in 2010. In 2015, he received the Ph.D. degree in Electrical and Computer Engineering from Brigham Young University in Provo, UT. Currently he leads the radar systems research group at Wavetronix, in Provo, UT.

In 2009, Dr. Mehmood was a recipient of the IEEE AP-S Undergraduate Research Award. In 2012, he was awarded the Brigham Young University High Impact Doctoral Research Assistantship Award. Dr. Mehmood's current research interests include over-the-air testing, reconfigurable antennas, optimization techniques, MIMO communications and radar, and physical layer security.